sustainability

MDPI

Article

Long-Term Wind–Wave Climate and Integrated Metocean Screening for Offshore Wind Development in the Binh Thuan–Phu Quy Offshore Domain, Vietnam

Thanh Dam Pham [1,2,*], Thanh Binh Dinh [1,3], Duy Manh Le [1,3], Du Van Toan [4], Pham Quy Ngoc [5] and Dong Trong Nguyen [6]

[1] Laboratory of Advanced Materials and Natural Resources, Institute for Advanced Study in Technology, Ton Duc Thang University, Ho Chi Minh City 700000, Vietnam; dinhthanhbinh@tdtu.edu.vn (T.B.D.); leduymanh@tdtu.edu.vn (D.M.L.)
[2] Faculty of Electrical and Electronics Engineering, Ton Duc Thang University, Ho Chi Minh City 700000, Vietnam
[3] Faculty of Applied Sciences, Ton Duc Thang University, Ho Chi Minh City 700000, Vietnam
[4] Institute of Meteorology, Hydrology, Environmental and Marine Sciences, Ministry of Agriculture and Environment, Hanoi 100000, Vietnam; dvtoan@mae.gov.vn
[5] Vietnam Petroleum Institute, Hanoi 100000, Vietnam; ngocpq@vpi.pvn.vn
[6] Department of Marine Technology, Norwegian University of Science and Technology (NTNU), 7491 Trondheim, Norway; dong.t.nguyen@ntnu.no
* Correspondence: phamthanhdam@tdtu.edu.vn

Abstract

Offshore wind development in the Binh Thuan–Phu Quy offshore domain requires regional, multi-variable preliminary metocean screening that extends beyond wind-resource mapping alone. This study presents a 32-year integrated wind–wave–bathymetry screening of four representative offshore wind sites in the Binh Thuan–Phu Quy offshore domain, Vietnam, using hourly ERA5 reanalysis data (1993–2024) and GEBCO 2025 bathymetry. The sites span four water-depth classes: shallow nearshore (BT01, 27 m), bottom-fixed (BT02, 49 m), transitional (BT03, 81 m), and floating-suitable (BT04, 161 m). For the IEA Wind 15 MW reference turbine at 150 m hub height, mean wind speed increases from 7.71 m s^{-1} at BT01 to 9.75 m s^{-1} at BT04, gross single-turbine capacity factor from 46.7% to 62.2%, and gross annual energy production from 61.4 to 81.7 GWh yr^{-1}. Along the selected BT01–BT04 sequence, mean significant wave height increases from 1.06 m to 1.49 m, with P95 H_s rising from 2.15 to 3.27 m. The northeast monsoon (November–March) dominates both wind and wave energy at all sites, whereas the mildest sea states occur during the April–May transition months. These conditions identify April–May as having the lowest monthly mean sea states; monthly means alone do not define operational weather windows. Interannual variability of annual gross capacity factor is moderate, with coefficients of variation of 9.8–10.2%. The integrated screening matrix shows that wind resource, energy yield, water depth, and wave exposure increase together along the selected four-site sequence, without implying a causal depth relationship or a domain-wide trend: the highest-yield site requires a floating substructure under the most exposed conditions, whereas the most benign site yields the least energy. All reported values are gross, reanalysis-based screening indicators rather than bankable resource estimates. From a sustainability perspective, the framework supports balanced early-stage planning by considering energy yield together with depth and marine exposure, while its open, long-term datasets provide reproducible, comparatively low-cost decision support for data-scarce emerging offshore wind markets. It does not quantify lifecycle, ecological, social, or economic sustainability.

Check for updates

Academic Editors: Alexandra Ionelia Diaconita and Gabriel Andrei

Received: 9 July 2026
Revised: 26 July 2026
Accepted: 29 July 2026
Published: 6 August 2026

Keywords: offshore wind resource; metocean screening; ERA5 reanalysis; wave climate; monsoon seasonality; sustainable offshore wind planning

1. Introduction

Offshore wind has moved from a niche technology to a mainstream component of global power-system decarbonization. According to the Global Wind Energy Council, cumulative installed offshore wind capacity worldwide reached approximately 75 GW by the end of 2023, with deployment increasingly extending beyond the North Sea into East and Southeast Asian waters [1–3]. This expansion has been accompanied by rapid turbine upscaling: commercial offshore turbines in the 14–16 MW class are now entering service, and openly documented reference designs such as the International Energy Agency (IEA) Wind 15 MW and 22 MW turbines provide common benchmarks for resource and design studies [4–6]. Because individual projects now represent multi-billion-dollar capital commitments, robust early-stage characterization of the offshore environment has become a prerequisite for project planning, and long-term hourly metocean databases—covering wind resource, wave climate, and bathymetry—are routinely required to support site screening, gross energy-yield estimation, foundation-type selection, and project preparation [1,7].

Reliable offshore wind resource characterization rests on a small set of interrelated metrics. Mean wind speed and its vertical extrapolation to hub height [8], wind power density (WPD), and turbine-specific capacity factor (CF) jointly determine gross energy yield, while the two-parameter Weibull distribution remains the standard statistical model for the wind-speed frequency distribution in energy applications [9,10]. Equally important are the temporal dimensions of the resource: monsoon-driven seasonality controls the intra-annual distribution of production, and interannual variability of the wind climate translates directly into uncertainty in annual energy production (AEP) and project revenue [11]. Capturing these low-frequency signals requires records substantially longer than the few years typically available from measurement campaigns or limited-period mesoscale simulations; multi-decadal assessments, such as the 55-year analysis of the southern Chinese coast by Wen et al. [12], have demonstrated the value of long records in constraining interannual and decadal variability. In practice, atmospheric reanalyses—and the fifth-generation reanalysis of the European Center for Medium-Range Weather Forecasts (ECMWF), ERA5, in particular [13,14]—have become widely used as a basis for such long-term assessments, offering consistent hourly wind and wave fields over several decades, with documented skill and known limitations for wind-energy applications [15,16].

Wind-only assessments are nevertheless insufficient for offshore wind development decisions. Water depth determines the applicable foundation technology—monopile, jacket, or floating substructure—and exerts a dominant influence on capital cost, with floating concepts required beyond roughly 60–80 m depth at substantially higher present-day cost [7,17,18]. The wave climate governs structural loading, installation and access conditions, vessel accessibility, and the fraction of time during which operation and maintenance activities can be performed; significant wave height and wave period, therefore, enter directly into logistics planning and availability estimates. Long-term ERA5-based wave climatologies for the broader region show pronounced monsoonal modulation of the wave field [19], implying that the seasons of highest energy production may coincide with the most restricted marine access. Recognizing these couplings, recent site-selection frameworks explicitly combine wind resource with water depth, wave exposure, and other spatial constraints in multi-criteria analyses [20–22]. An integrated wind–wave–bathymetry perspective is, therefore, a minimum requirement for meaningful early-stage screening.

Sustainable offshore wind development requires more than maximizing wind speed or energy yield. Water depth, indicative foundation demand, wave exposure, installation constraints, marine access, and maintenance conditions should be considered early so that limited survey and planning resources are not directed toward poorly matched locations. Integrated open-data screening can support transparent and resource-efficient prioritization in data-scarce markets, while remaining only a precursor to environmental, socio-economic, lifecycle, techno-economic, and marine-spatial assessments.

Vietnam has been widely identified as a promising offshore wind market in Southeast Asia, owing to its long coastline, monsoon-driven wind climate, and extensive shallow-to-deep offshore areas suited to a range of bottom-fixed and floating technologies [2,3,7]. National power planning—the Power Development Plan VIII (PDP8) and its 2025 revision—provides policy motivation for offshore wind development in Vietnam, setting national ambitions of tens of gigawatts of installed capacity over the coming decades [23,24]; such planning targets, however, do not by themselves supply the regional metocean evidence that early-stage project screening requires. Within Vietnamese waters, the south-central offshore region—particularly the offshore waters of the former Binh Thuan coastal region and the waters surrounding Phu Quy Island—has been repeatedly identified in the scientific literature as a promising area for early commercial-scale development, owing to consistent monsoonal winds, a moderate continental-shelf gradient, and proximity to major load centers in southern Vietnam [25–28]. A growing body of studies underpins this assessment, but each addresses only part of the information required for site screening. Using 10 km Weather Research and Forecasting (WRF) simulations validated against observations from Phu Quy Island and other coastal locations, Doan et al. [25] reported very high offshore wind speeds near Phu Quy Island; however, the study was limited to a comparatively short simulation period and considered wind only. Numerical simulation of the offshore wind potential along the southern coast is further described by Doan et al. [29] with a similar wind-only scope. At the national level, Quang et al. [26] applied cross-calibrated multi-platform satellite winds with an 8 MW reference turbine, and Tuy et al. [27] combined WRF downscaling with Sentinel-1 satellite-derived winds to map optimal sites and estimate annual energy production; both provide valuable national-scale zoning but operate at coarse spatial granularity relative to project needs, rely on now-superseded turbine classes, and include neither wave climate nor bathymetric characterization. Regional climate-projection studies [30,31] address future resource evolution rather than present-day engineering screening. Most recently, a 3 km WRF-based national atlas [28] quantified theoretical and technical offshore wind potential, yet remains a wind-resource product without integrated wave or foundation-depth information. Wave-energy studies for the central Vietnamese coast [32] treat the wave field in isolation from wind development. In summary, the existing literature is characterized by limited temporal coverage, national rather than representative-coordinate focus, wind-only assessment, and the limited integration of wave and bathymetric information within a single integrated regional screening framework.

Consequently, although several studies have investigated offshore wind resources in Vietnamese waters, a multi-decadal, development-oriented database that integrates wind resource, wave climate, and bathymetric characteristics at representative engineering sites in the Binh Thuan–Phu Quy offshore domain remains unavailable in the peer-reviewed literature—particularly one referenced to a current-generation 15 MW turbine and modern global bathymetry.

This study addresses that gap. Specifically, it aims to: (i) develop a long-term (1993–2024) hourly offshore wind and wave database for the Binh Thuan–Phu Quy offshore domain from ERA5 reanalysis [13]; (ii) characterize the spatial and temporal variation of wind speed, wind power density, significant wave height, and peak wave period across the domain, including monsoon seasonality and interannual variability; (iii) evaluate four representative offshore locations spanning shallow, bottom-fixed, transitional, and floating depth classes—characterizing the wind-speed distribution through Weibull statistics and wind roses, and computing gross CF directly from the hourly time series with the power curve of the IEA Wind 15 MW reference turbine [4], with sensitivity to selected reference turbine sizes [5,33,34] and (iv) integrate wind resource, wave climate, and 2025 bathymetry from the General Bathymetric Chart of the Oceans (GEBCO) [35] into a metocean screening matrix that links water depth to indicative foundation classes and supports early-stage prioritization of development areas.

This study does not introduce a new analytical method: the wind- and wave-resource metrics, Weibull fitting, and gross capacity-factor calculations all follow established, widely used approaches. Its contribution is an integrated, regional, long-term wind–wave–bathymetry preliminary screening workflow, applied consistently across four representative depth classes in the Binh Thuan–Phu Quy offshore domain—a data-scarce setting in which wind, wave, and bathymetric information have rarely been brought together within a single representative-coordinate assessment. Beyond its immediate use for offshore wind planning and site screening in one of Vietnam's priority development regions, the resulting database and screening workflow provide a basis for subsequent, more detailed studies on extreme metocean conditions and environmental contours, wind–wave–current misalignment, wake effects and farm-level energy yield, and marine spatial planning. The study deliberately does not perform extreme-value analysis, ocean-current characterization, environmental contour estimation, or formal design-load-case development following the standards of the International Electrotechnical Commission (IEC) for fixed and floating offshore wind systems [36,37]; these remain necessary follow-up steps for any site progressing beyond the early-stage, screening-level assessment presented here (Section 4). Its sustainability contribution is, therefore, limited to transparent, resource-efficient early decision support: the screening matrix exposes yield–depth–exposure trade-offs but does not measure sustainability outcomes.

The paper is organized as follows. Section 2 describes the study domain, data sources, and analytical methodology. Section 3 presents results for each objective. Section 4 discusses the scientific contribution, key trade-offs, and limitations of the screening. Section 5 summarizes the main findings.

2. Data and Methods

2.1. Study Area and Representative Screening Sites

The study domain extends from 9.5 to 11.5° N and 108.2 to 109.6° E across the Binh Thuan–Phu Quy offshore region, encompassing the offshore waters between the south-central mainland coast and Phu Quy Island (Figure 1). The domain covers an area of approximately 220 km × 155 km, spanning the inner continental shelf adjacent to the mainland coast, the waters surrounding Phu Quy Island, and the transition to intermediate-depth offshore waters. The atmospheric and oceanographic conditions of the domain are dominated by the East Asian monsoon system, alternating between a northeast (NE) monsoon phase during boreal winter and a southwest (SW) monsoon phase during boreal summer, with transition periods of shifting or weakened winds [38,39].

Four representative screening sites were selected to span a depth gradient from the inner continental shelf to waters suitable for floating offshore wind (Table 1):

- BT01 —10.75° N, 108.35° E; water depth 27 m; shallow nearshore depth class.
- BT02—10.15° N, 108.30° E; water depth 49 m; bottom-fixed depth class.
- BT03—9.95° N, 108.70° E; water depth 81 m; transitional depth class.
- BT04—10.40° N, 109.30° E; water depth 161 m; floating-suitable depth class.

Table 1. Representative screening sites and GEBCO 2025 water depth. Sites were selected to span four foundation-class depth bands. BT02 and BT03 map to the same nearest ERA5 0.5° wave grid cell; wave statistics at all four sites are obtained by bilinear interpolation over the surrounding valid (non-land-masked) ocean grid cells to provide coordinate-specific estimates (Section 2.7); interpolation does not increase ERA5's native resolution. Phu Quy Island is a geographic reference location for the domain; its meteorological station data are not used in this study.

Site	Lat (°N)	Lon (°E)	Role	Depth (m)	Depth Class
BT01	10.75	108.35	Shallow nearshore	27	Shallow (<30 m)
BT02	10.15	108.30	Bottom-fixed offshore	49	Bottom-fixed (30–60 m)
BT03	9.95	108.70	Transitional depth	81	Transitional (60–100 m)
BT04	10.40	109.30	Floating-suitable	161	Floating (>100 m)
Phu Quy	10.52	108.93	Geographic reference	Not applicable	Island

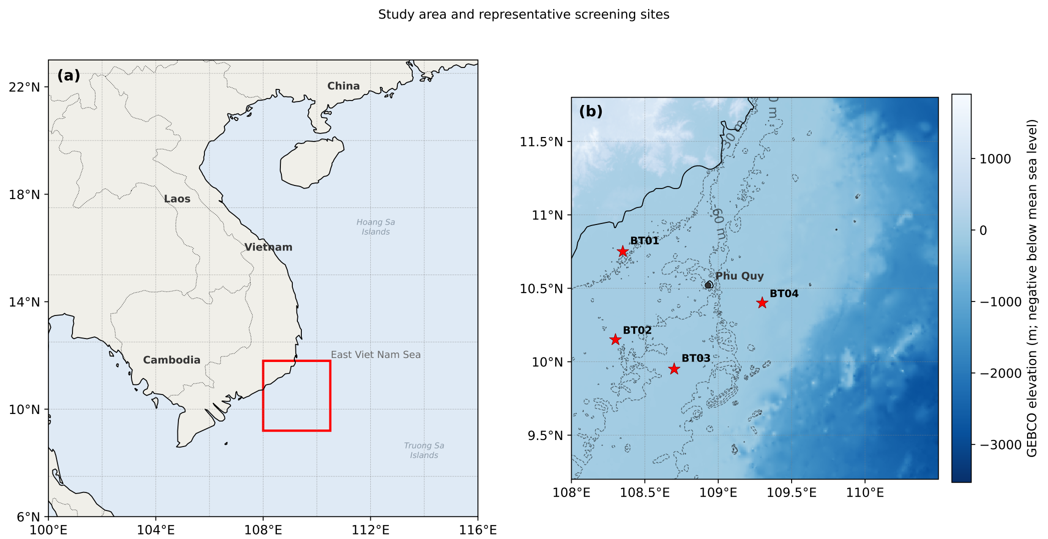

Figure 1. Study domain and bathymetry. (**a**) Regional map showing the location of the Binh Thuan–Phu Quy offshore domain off the south-central coast of Vietnam; the red rectangle marks the detailed study area. (**b**) Zoomed bathymetric map of the study area based on GEBCO 2025, showing the four representative screening sites BT01–BT04 and Phu Quy Island as a geographic reference. Contour lines at 30, 60, and 100 m indicate indicative foundation-depth classes. Negative elevation values represent water depth below mean sea level.

Sites were positioned to fall within the ERA5 wind analysis bounding box, to avoid land-contaminated ERA5 wave cells where possible, and to span the spatial and bathymetric gradient from nearshore to open-ocean offshore conditions. The selection was constrained to representative points located within broad, locally coherent bathymetric zones rather than isolated seabed features, so that the extracted GEBCO depth is indicative of the surrounding depth class rather than a single grid-cell anomaly. At the native 0.5° ERA5 wave grid resolution, BT02 and BT03 fall in the same nearest wave grid cell; wave statistics for all four sites are, therefore, obtained by bilinear interpolation over the surrounding valid ocean grid cells (Section 2.7) rather than simple nearest-cell snapping. These are coordinate-specific estimates from the native coarse field, not resolved local conditions. The Phu Quy Island location (10.52° N, 108.93° E) is shown as a geographic reference on the study domain map (Figure 1); it is not a development screening site, and station observations from this location are not used in this study. These sites are designated representative screening sites; they do not constitute a final site selection.

2.2. ERA5 Reanalysis Data

Wind and wave data were sourced from the ERA5 global atmospheric reanalysis [13], produced by ECMWF under the Copernicus Climate Change Service (C3S). ERA5 provides hourly estimates of atmospheric and ocean-wave variables with native horizontal resolution of approximately 31 km; single-level products are distributed on regular grids of 0.25° (atmosphere) and 0.5° (waves). Although the complete ERA5 record extends from 1940 to the present [14,40], this study uses the period 1 January 1993 to 31 December 2024—a continuous hourly record of 32 years—to ensure consistency with the post-1993 era of comprehensive satellite ocean-altimeter data assimilation.

The following ERA5 variables were extracted over the full study domain and at each representative screening site:

- Zonal (u_{10}, u_{100}) and meridional (v_{10}, v_{100}) wind components at 10 m and 100 m above the surface (0.25° grid; hourly; 1993–2024).
- Significant wave height (H_s), peak spectral wave period (T_p), mean wave period (T_m), and mean wave direction (MWD) (0.5° grid; hourly; 1993–2024).

The data sources are summarized in Table 2.

Table 2. Data sources used in this study. NREL: National Renewable Energy Laboratory; DTU: Technical University of Denmark; IEA: International Energy Agency.

Dataset	Variables	Resolution	Period	Source
ERA5 atmosphere	u_{10}, v_{10}, u_{100}, v_{100}	0.25°, hourly	1993–2024	ECMWF
ERA5 waves	H_s, T_p (`pp1d`), T_m (`mwp`), MWD	0.5°, hourly	1993–2024	ECMWF
GEBCO bathymetry	Elevation	15 arc-sec	Static	GEBCO 2025
Power curves	$P(V)$, 5/10/15/22 MW	Not applicable	Not applicable	NREL; DTU/IEA

ERA5 has been widely evaluated against in-situ wind and wave measurements and is commonly used for offshore energy screening studies [15,16]. In an evaluation using regional buoy observations, Wang and Wang [41] reported correlation coefficients of 0.87–0.93 between ERA5 significant wave heights and in-situ buoy data. These published evaluations support the use of ERA5 for preliminary screening, but they do not replace site-specific validation. The uncertainty of ERA5-derived hub-height wind speeds in this domain, and the interpretation of published WRF validation results near island stations, are discussed in Section 4.5.

Wind speed magnitude at each reference height is computed as follows:

$$V_{10}(t) = \sqrt{u_{10}^2(t) + v_{10}^2(t)}, \qquad V_{100}(t) = \sqrt{u_{100}^2(t) + v_{100}^2(t)} \tag{1}$$

Wind direction (meteorological convention: direction from which the wind blows, measured clockwise from north) is computed from the ERA5 10 m wind components as follows:

$$\theta(t) = \left[\operatorname{atan2}\left(-u_{10}(t), -v_{10}(t)\right) \cdot \frac{180}{\pi} + 360\right] \bmod 360^\circ \tag{2}$$

The same meteorological-direction convention and equation were applied to u_{100} and v_{100} when 100 m wind directions were required for the seasonal classification.

2.3. GEBCO 2025 Bathymetry

Bathymetric information is taken from the GEBCO 2025 grid, produced by the Nippon Foundation–GEBCO Seabed 2030 Project [35]. The GEBCO 2025 grid provides a continuous global terrain model on a 15 arc-second (≈460 m at the equator) latitude–longitude grid. For this study, the GEBCO 2025 data are subset to the bounding box 9.0–12.0° N, 107.75–110.0° E (wider than the ERA5 analysis domain to avoid edge effects in visualization). The bathymetry is used: (i) to determine the representative water depth at each screening site; (ii) to support spatial visualization of the depth environment alongside wind and wave resource maps (Figure 1) and (iii) to contextualize each site within a depth class relevant to foundation technology. Water depths at the four screening sites are taken from the GEBCO 2025 grid at the exact site coordinates (Table 1).

2.4. Wind Speed, Wind Direction, and Hub-Height Extrapolation

Hub-height wind speed at each screening site was derived from ERA5 wind components in two steps. First, a time-varying power-law shear exponent was computed at each site from hourly ERA5 wind speeds at 10 m and 100 m:

$$\alpha(t) = \frac{\ln[V_{100}(t)\ /\ V_{10}(t)]}{\ln(100/10)} \tag{3}$$

Values of α were quality-controlled by excluding time steps where V_{10} or V_{100} were below 0.5 m s^{-1}, and by replacing α values outside the range $[-0.20,\ 0.60]$ with the monthly median value at the same site. Site-specific time-varying α values are used rather than a fixed constant, following the global analysis of Jung and Schindler [8]. Second, hub-height wind speed for turbine hub height H was computed as follows:

$$V_{\text{hub}}(t) = V_{100}(t)\left(\frac{H}{100}\right)^{\alpha(t)} \tag{4}$$

For the IEA Wind 15 MW reference turbine (hub height 150 m), $H = 150$ m. Hub heights for the sensitivity turbines are NREL 5 MW: 90 m; DTU/IEA 10 MW: 119 m; and IEA 22 MW: 170 m. This extrapolation is an ERA5-based, coordinate-specific power-law approximation for screening purposes; it is not an IEC-compliant power-performance measurement and does not resolve local stability, turbulence, or mesoscale coastal effects.

Alpha QC diagnostics were tabulated annually, by calendar month, and by season, including the fractions with $V_{10} < 0.5$ m s^{-1}, $V_{100} < 0.5$ m s^{-1}, $\alpha < -0.20$, $\alpha > 0.60$, and the total fraction replaced. Four extrapolation cases were compared: (A) the baseline hourly alpha with bounds $[-0.20, 0.60]$ and monthly-median replacement; (B) fixed $\alpha = 0.10$; (C) fixed $\alpha = 1/7$ and (D) hourly alpha with alternative bounds $[-0.10, 0.40]$ and the same replacement logic. For each case and coordinate, mean wind at 150 and 170 m and gross CF/AEP for the IEA 15 and 22 MW references were recomputed. These cases quantify sensitivity to the extrapolation method; they are not probabilistic confidence intervals.

2.5. Weibull Distribution and Wind Power Density

A two-parameter Weibull probability density function was fitted to the hub-height wind speed time series at each site using maximum-likelihood estimation with the location parameter fixed at zero [9,10]:

$$f(v) = \frac{k}{c}\left(\frac{v}{c}\right)^{k-1} \exp\left[-\left(\frac{v}{c}\right)^{k}\right] \tag{5}$$

where v is wind speed (m s^{-1}), k is the dimensionless shape parameter, and c is the scale parameter (m s^{-1}).

WPD was computed from the hourly hub-height wind speed time series as follows:

$$\mathrm{WPD_{ts}} = \frac{1}{2}\,\rho\,\overline{V_{\mathrm{hub}}^{3}} \tag{6}$$

and from the fitted Weibull distribution as follows:

$$\mathrm{WPD_{W}} = \frac{1}{2}\,\rho\,c^{3}\,\Gamma\!\left(1+\frac{3}{k}\right) \tag{7}$$

where $\rho = 1.225\ \mathrm{kg\,m^{-3}}$ is standard air density and Γ is the gamma function. The Weibull-based estimate (Equation (7)) serves only as an internal cross-check on the quality of the distributional fit. All WPD values reported in this paper are computed directly from the hourly time series (Equation (6)), and all energy calculations (Section 2.6) operate on the hourly hub-height wind speed time series with turbine power curves; the fitted Weibull distribution is not used in any energy computation.

2.6. Turbine Power Curves and Gross AEP/CF Calculation

Hourly gross power output was computed by linearly interpolating hub-height wind speed against the published power curve $P(V)$ of each reference turbine. For wind speeds below cut-in and above cut-out, turbine power was set to zero; between tabulated power-curve points, linear interpolation was applied, and power was capped at the rated value where applicable. Four power curves were used:

- NREL 5 MW, hub height 90 m [33]
- DTU/IEA 10 MW reference turbine, hub height 119 m [34]
- IEA Wind 15 MW, hub height 150 m [4]—manuscript baseline
- IEA Wind 22 MW, hub height 170 m [5]

Gross AEP and gross single-turbine CF were computed from the full ERA5 record as follows:

$$\overline{P} = \frac{\sum\limits_{i\in\mathcal{V}} P[V_{\mathrm{hub}}(t_i)]\Delta t_i}{\sum\limits_{i\in\mathcal{V}} \Delta t_i}, \qquad \mathrm{AEP_{mean}} = \overline{P}\,(8760\ \mathrm{h\,yr^{-1}}), \tag{8}$$

$$\mathrm{CF_{gross}} = \frac{\overline{P}}{P_{\mathrm{rated}}} = \frac{\mathrm{AEP_{mean}}}{P_{\mathrm{rated}}(8760\ \mathrm{h\,yr^{-1}})}. \tag{9}$$

Here, $\mathcal{V}$ is the set of valid hourly samples, $\Delta t_i = 1$ h, and P_{rated} is the turbine rated power (MW). Mean power $\overline{P}$ is calculated from all valid hourly records and is normalized to 8760 $\mathrm{h\,yr^{-1}}$ to obtain mean annual AEP. Hours from leap years, therefore, contribute valid samples to the long-term mean power but do not increase the fixed 8760 h annual normalization. All capacity factors reported in this paper are gross, single-turbine values. They exclude wake losses, electrical transmission losses, turbine availability derating, curtailment, and long-term degradation. They represent an upper-bound, resource-based indicator for a single turbine; they are not estimates of wind-farm-level output.

2.7. ERA5 Wave Data and Land-Masking

ERA5 wave fields are computed on a 0.5° grid. In this coastal domain, nearest-grid-point extraction is sensitive to the ERA5 wave land–sea mask, and BT02 and BT03 share the same nearest valid ocean grid cell (10.2° N, 108.5° E). Simple nearest-valid-cell snapping would, therefore, assign identical wave statistics to BT02 and BT03 and cannot establish a local site-to-site wave gradient. For the baseline, wave statistics at each coordinate are obtained by bilinear interpolation over the surrounding 0.5° grid cells: land-masked corner cells (all-NaN) are dropped and the remaining bilinear weights are renormalized among the valid ocean corners. Where all four surrounding cells are land-masked, the nearest valid ocean cell is used instead. A dedicated quality-control comparison also evaluated nearest-valid-cell and inverse-distance weighting over valid surrounding corners. Nearest extraction assigns identical statistics to BT02 and BT03, whereas bilinear and inverse-distance estimates differ; consequently, their separation is extraction-method dependent, not resolved island sheltering or refraction. Interpolation provides coordinate-specific estimates from the native coarse field and cannot resolve local island sheltering, coastal refraction, or bathymetric wave transformation. For transparency, the four enclosing grid coordinates, land/ocean validity, corner mean and P95 H_s, original bilinear weights, and weights renormalized after land masking were retained. Three extraction methods were compared: the nearest valid ocean cell; masked bilinear interpolation and inverse-distance weighting of valid enclosing ocean cells, using inverse squared coordinate distance. Method-dependent ranges and rank changes were reported rather than selecting the method that produced a desired site separation. The peak spectral wave period (T_p, ERA5 variable `pp1d`) is used at all four sites; the mean wave period (T_m, ERA5 variable `mwp`) would be used as a fallback at any site where `pp1d` is entirely missing (all-NaN) across the interpolated cells, but this did not occur for any of the four sites under bilinear interpolation.

Wave statistics reported include the following: long-term mean H_s, 95th-percentile H_s (P95 H_s), maximum H_s, mean peak or mean wave period, MWD, and interannual coefficient of variation (COV) of annual mean H_s. The 95th-percentile H_s is a long-term climate indicator derived from the full 1993–2024 record. It is not an extreme design condition; estimation of return-period wave heights requires separate extreme-value analysis and is reserved for follow-up studies.

2.8. Monsoon Seasonality and Interannual Variability

A data-driven seasonal classification was adopted based on monthly circular wind-direction statistics derived from hourly ERA5 wind data at the four screening sites over 1993–2024. For each calendar month and site, the circular mean meteorological wind direction and resultant vector length $R \in [0, 1]$ were computed from ERA5 100 m wind components using the convention in Equation (2). Months were grouped according to the combination of mean direction sector and directional persistence observed consistently across the four sites. November–March showed persistent northeasterly flow and were classified as the NE monsoon; June–September showed persistent southwesterly to west-southwesterly flow and were classified as the SW monsoon; April, May, and October showed weaker or shifting directional persistence and were classified as transition months. The BT04 resultant lengths provide an offshore reference example of this separation, with $R > 0.80$ during the core NE monsoon, $R > 0.71$ during the SW monsoon, and $R < 0.55$ during transition months. This classification yields the following:

- NE monsoon: November–March (months 11, 12, 1, 2, 3)
- SW monsoon: June–September (months 6, 7, 8, 9)
- Transition: April, May, and October (months 4, 5, 10)

The classification derivation and its site-specific justification are presented in Section 3.5. Monthly climatologies of hub-height wind speed, gross capacity factor, and significant wave height were computed by averaging across all 32 years of the 1993–2024 record. Seasonal statistics were computed by aggregating hourly ERA5 data within each season. For annual statistics, an enforced threshold of at least 8000 valid hourly records per calendar year was applied. For monthly statistics, each year–month was required to contain at least 75% of its expected hourly records. Periods below either threshold were retained in the completeness records and explicitly flagged and masked from the corresponding aggregate, rather than being silently dropped. All site-years and site-year–months in the 1993–2024 analysis satisfied these thresholds.

Interannual variability was characterized by COV of annual means, computed as follows:

$$\text{COV} = \frac{\sigma_{\text{annual}}}{\mu_{\text{annual}}} \times 100\% \quad (10)$$

where σ_{annual} is the interannual standard deviation of annual means and μ_{annual} is the long-term mean of those annual values. COV was computed for annual mean hub-height wind speed, annual gross CF, annual wind power density, and annual mean H_s at each site over the 32-year ERA5 record. Monotonic trends were tested using the two-sided Mann–Kendall statistic, with Sen's slope and its 95% confidence interval. Pettitt's rank-based test was used to screen for a single change point. Significance was assessed at $\alpha = 0.05$. These diagnostics are distinct from COV: COV measures interannual dispersion, whereas the tests address monotonic change and an abrupt distributional shift, respectively.

2.9. Integrated Metocean Screening Framework

The final step of the workflow combines the outputs above into a compact integrated metocean screening matrix for sites BT01–BT04. Each site is characterized by water depth and indicative foundation class, long-term mean hub-height wind speed, gross capacity factor (IEA 15 MW baseline), interannual dispersion of production (COV of gross CF), and mean and 95th-percentile H_s. The screening matrix supports early-stage engineering prioritization. It does not constitute a final site selection and does not claim bankable resource estimates or design-ready metocean conditions. All computations were performed in Python 3.11.9 using `xarray`, `NumPy`, `SciPy`, `pandas`, `matplotlib`, and `cartopy`, with inputs drawn from publicly available ERA5 [13] and GEBCO 2025 [35].

2.10. Combined Screening-Sensitivity Framework

The four wind-extrapolation cases were cross-compared with the three wave-extraction methods at each coordinate. The assessment reports ranges of mean V_{hub}, gross 15 MW CF and AEP, mean and P95 H_s, together with separate wind-resource and wave-exposure ranks. Rank invariance and BT02–BT03 order exchanges were checked explicitly. No weighted multi-criteria score was introduced, and the resulting method-based ranges are not presented as a formal total uncertainty budget.

3. Results

3.1. Study Domain and Bathymetry

Across the Binh Thuan–Phu Quy offshore domain, bathymetry shows a systematic depth gradient from the inner shelf to deeper offshore waters (Figure 1). GEBCO 2025 bathymetry confirms water depths of 27 m (BT01), 49 m (BT02), 81 m (BT03), and 161 m (BT04) at the four representative screening sites (Table 1), spanning four distinct foundation-class categories: shallow (<30 m), bottom-fixed (30–60 m), transitional (60–100 m), and floating-suitable (>100 m). The four sites, therefore, provide a representative depth-gradient sequence from shallow nearshore to floating-depth conditions within the same regional wind–wave setting. This sequence allows first-order comparisons of wind resource, wave exposure, gross energy yield, and foundation-depth implications across depth classes, while recognizing that the sites are screening points rather than an optimized development transect.

3.2. Spatial Wind Resource at Hub Height

Mean hub-height wind speed at 150 m increases along the selected BT01–BT04 sequence, from 7.71 $\text{m}\,\text{s}^{-1}$ (BT01, 27 m) to 9.75 $\text{m}\,\text{s}^{-1}$ (BT04, 161 m; Table 3; Figure 2), with BT02 (9.04 $\mathrm{m\,s^{-1}}$) and BT03 (9.30 $\mathrm{m\,s^{-1}}$) at intermediate depths. This pattern is reported as co-variation across the selected coordinates and is not interpreted as an independent effect of water depth, distance from shore, or coastal exposure. Wind power density (WPD) at 150 m, computed directly from the hourly time series (Equation (6)), follows the same gradient, from 452.6 $\mathrm{W\,m^{-2}}$ (BT01) to 957.5 $\mathrm{W\,m^{-2}}$ (BT04). Weibull maximum-likelihood fits yield shape parameters $k = 2.18$–2.34 and scale parameters $c = 8.67$–10.98 $\mathrm{m\,s^{-1}}$ (Table 3); these fitted parameters characterize the wind-speed distribution and serve as a distributional cross-check only—all WPD, AEP, and CF values in this paper are computed directly from the hourly time series (Section 2.6). Mean time-varying power-law shear exponents ($\bar{\alpha} = 0.056$–0.076) decrease with distance from shore, consistent with the reduced influence of coastal surface roughness over deeper open-ocean water; these exponents are ERA5-derived, screening-level estimates and are not interpreted further in terms of local boundary-layer stability.

Table 3. Wind resource statistics and gross single-turbine energy yield for the IEA Wind 15 MW reference turbine (hub height 150 m, rated power 15 MW). WPD, AEP, and CF are computed directly from the hourly hub-height time series (Equations (6) and (8)); Weibull k and c are distributional fit parameters reported for reference. All CF and AEP values are gross (no wake, electrical, or availability losses). COV = interannual coefficient of variation of annual gross CF.

Site	$\bar{V}_{\mathrm{hub}}$ ($\mathrm{m\,s^{-1}}$)	k	c ($\mathrm{m\,s^{-1}}$)	WPD ($\mathrm{W\,m^{-2}}$)	AEP ($\mathrm{GWh\,yr^{-1}}$)	CF (%)	$\mathrm{COV_{CF}}$ (%)
BT01	7.71	2.34	8.67	452.6	61.4	46.70	10.23
BT02	9.04	2.28	10.19	748.5	75.6	57.52	9.88
BT03	9.30	2.18	10.48	843.2	77.0	58.56	10.18
BT04	9.75	2.21	10.98	957.5	81.7	62.20	9.83

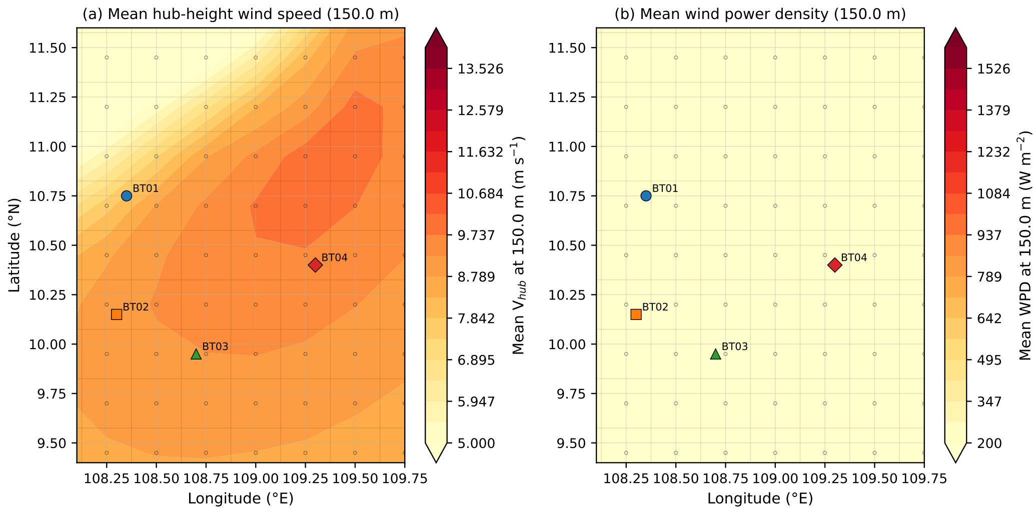

Figure 2. Climatological mean hub-height (150 m) wind speed over the study domain (1993–2024), derived by coordinate-specific power-law extrapolation from ERA5 10 m and 100 m wind components. Open nodes and cell boundaries show the native 0.25° atmospheric grid; symbols indicate the representative coordinates. The continuous display is visual interpolation and does not imply finer physical resolution. Mean hub-height wind speeds at BT01–BT04 are 7.71, 9.04, 9.30, and 9.75 $\mathrm{m\,s^{-1}}$, respectively, (Table 3).

3.3. Gross Energy Yield: IEA 15 MW Baseline

Gross single-turbine AEP (IEA Wind 15 MW; hub height 150 m) increases along the selected sequence, from 61.4 $\mathrm{GWh\,yr^{-1}}$ (BT01) to 81.7 $\mathrm{GWh\,yr^{-1}}$ (BT04; Table 3). Gross single-turbine capacity factor likewise increases along this sequence from 46.70% (BT01) through 57.52% (BT02) and 58.56% (BT03) to 62.20% (BT04). This CF and AEP gradient directly follows the hub-height wind-resource gradient of Section 3.2. Notably, BT02 and BT03 differ by only about one percentage point in gross CF and 1.4 GWh yr^{-1} in gross AEP despite belonging to different depth classes (49 m bottom-fixed versus 81 m transitional)—a contrast with direct screening implications that is taken up in Section 3.9. Monthly gross CF profiles (Figure 3) show a clear northeast monsoon peak at all sites. Interannual COV of gross single-turbine CF is 9.8–10.2% (Table 3). All values are gross, single-turbine indicators; loss mechanisms and their interpretation are addressed in Section 4.

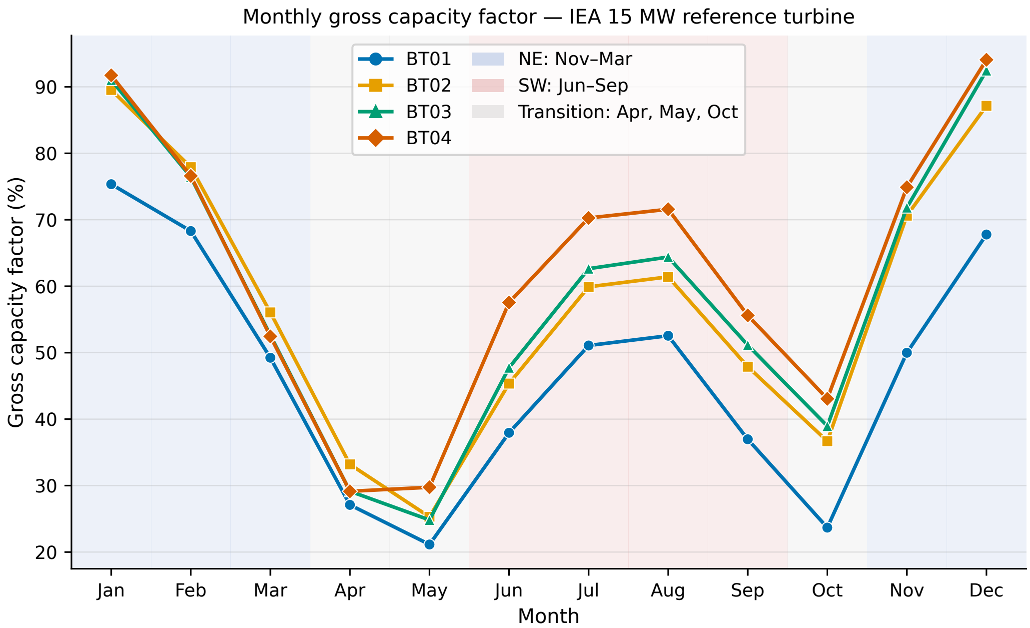

Figure 3. Monthly gross single-turbine capacity factor at BT01–BT04 for the IEA Wind 15 MW reference turbine (hub height 150 m), computed from ERA5 hourly hub-height wind speed over 1993–2024. Background shading indicates the NE monsoon (blue, November–March), SW monsoon (red, June–September), and transition months (grey, April, May, October). Values are gross upper-bound indicators (single turbine, no losses).

3.4. Wave Climate at the Representative Screening Sites

Mean significant wave height ($\bar{H}_s$), derived from bilinear interpolation of ERA5 wave fields to each coordinate, increases along the selected BT01–BT04 sequence from 1.06 m at BT01 to 1.49 m at BT04 (Table 4; Figure 4). This pattern describes the values obtained at the four selected coordinates and is not interpreted as a resolved regional or local wave gradient. BT02 and BT03 share the same nearest valid ERA5 0.5°wave grid cell (10.2° N, 108.5° E); nearest-valid-cell extraction would, therefore, have produced identical wave statistics for these two sites and cannot resolve a local wave-gradient difference. Bilinear interpolation over the surrounding valid-ocean grid cells instead produces distinct coordinate-specific estimates for BT02 (mean $H_s = 1.22$ m) and BT03 (mean $H_s = 1.39$ m). The 95th percentile of H_s (P95) ranges from 2.15 m (BT01) to 3.27 m (BT04). Maximum recorded H_s over the 1993–2024 period reaches 6.34 m at BT04; this is the largest hourly ERA5 value in the analysed record and should not be interpreted as an extreme return-period estimate. Mean peak wave period also increases along the selected sequence, from 5.96 s at BT01 to 6.86 s at BT04. Because the sites differ simultaneously in location, exposure, and surrounding bathymetry, the present ERA5 analysis does not attribute this variation to an individual physical mechanism. Taken together, the larger wave-climate indicators at the more exposed coordinates have screening-level implications rather than constituting quantified engineering or design results. Their effects on marine access, station-keeping, and structural loading would need to be established through subsequent operability and design-stage assessments. P95 H_s is used throughout as a climate-state indicator; it is not a return-period design wave height. Interannual COV of annual mean H_s is 5.8–6.5%, indicating limited interannual dispersion on multi-year timescales.

Table 4. Wave climate statistics at the four representative screening sites (ERA5, 1993–2024), obtained by bilinear interpolation of ERA5 wave fields to each site coordinate. $\bar{H}_s$: mean significant wave height; P95: 95th-percentile H_s; $H_{s,max}$: maximum recorded H_s; $\bar{T}_p$: mean peak spectral wave period; NE $\bar{H}_s$: NE monsoon mean (November–March); SW $\bar{H}_s$: SW monsoon mean (June–September). P95 H_s is a climate-state indicator, not an extreme design value.

Site	$\bar{H}_s$ (m)	P95 H_s (m)	$H_{s,max}$ (m)	$\bar{T}_p$ (s)	NE $\bar{H}_s$ (m)	SW $\bar{H}_s$ (m)
BT01	1.06	2.15	3.82	5.96	1.40	0.89
BT02	1.22	2.61	4.84	6.26	1.67	0.97
BT03	1.39	3.08	5.91	6.65	1.92	1.07
BT04	1.49	3.27	6.34	6.86	2.03	1.19

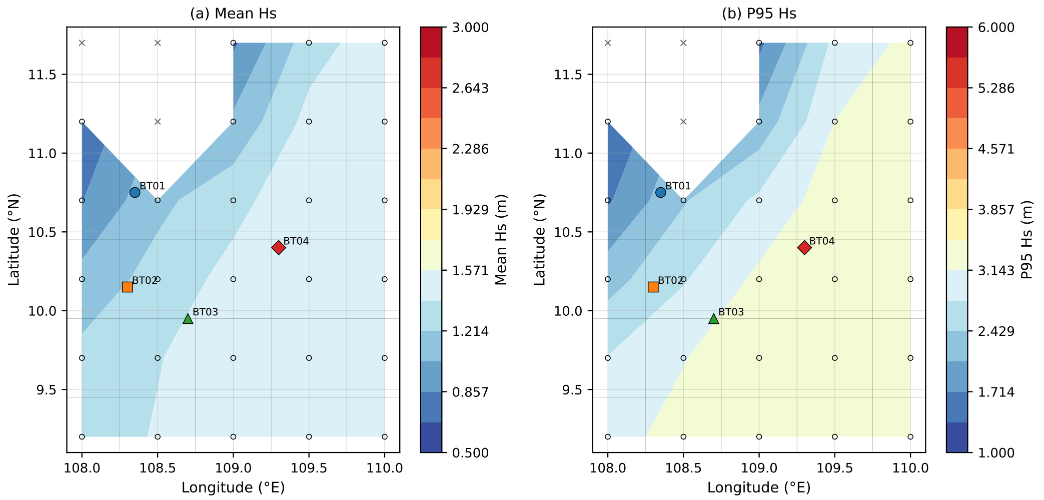

Figure 4. Wave climate at the four representative screening sites (ERA5, 1993–2024, bilinear interpolation). Mean annual significant wave height ($\bar{H}_s$) is 1.06, 1.22, 1.39, and 1.49 m at BT01–BT04, respectively. P95 H_s is a climate-state indicator; it is not an extreme structural design value. Native 0.5° wave nodes and cell boundaries are overlaid, with crosses for land-masked nodes. Interpolation supplies coordinate-specific estimates from the coarse field and does not resolve island sheltering, coastal refraction, or bathymetric wave transformation.

3.5. Monsoon Seasonality

Figure 5 shows the monthly circular mean meteorological wind direction and directional persistence (resultant length R) at all four sites over the ERA5 1993–2024 record. The figure reveals a clear three-season structure at all sites. November to March are characterized by persistent winds from the northeast sector ($R > 0.80$ at BT04), identifying these months as the core northeast (NE) monsoon season. June to September are characterized by persistent winds from the southwest to west-southwest sector ($R > 0.71$ at BT04), identifying these months as the southwest (SW) monsoon season. April, May, and October show substantially weaker directional persistence ($R < 0.55$ at BT04), with shifting mean directions, and are, therefore, classified as transition months. This data-driven three-season classification is consistent across all four sites and is used in all subsequent seasonal analyses (Section 2.8).

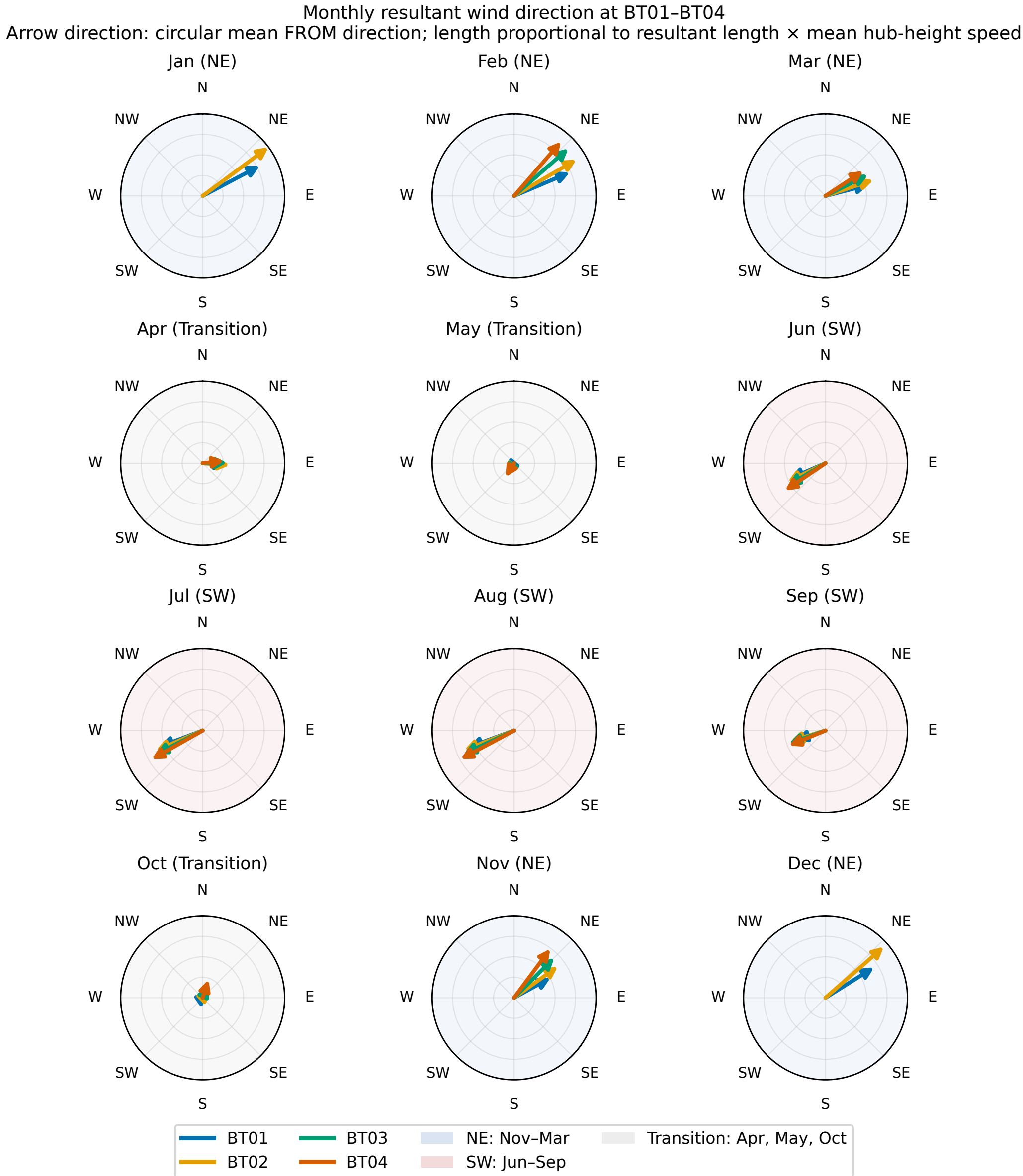

Figure 5. Monthly resultant wind direction at BT01–BT04 based on ERA5 hourly wind data for 1993–2024. Arrow direction represents the circular mean meteorological wind direction (FROM convention); arrow length is proportional to the product of resultant length R and mean hub-height wind speed. A longer, more aligned arrow indicates stronger directional persistence. The figure shows a persistent northeast monsoon regime from November to March, a southwest monsoon regime from June to September, and transition conditions with weaker, shifting winds in April, May, and October.

The NE monsoon (November–March) is the energetic season for both wind resource and wave forcing: it dominates wind energy and wave conditions simultaneously at all sites. Mean hub-height wind speed during the NE monsoon is $\bar{V}_{\text{hub}} = 9.15$–$12.02\ \text{m}\,\text{s}^{-1}$ across BT01–BT04, versus $\bar{V}_{\text{hub}} = 7.52$–$9.32\ \text{m}\,\text{s}^{-1}$ during the SW monsoon (June–September), a NE/SW ratio of 1.22–1.37 depending on site. Mean significant wave height during the NE monsoon is 1.40–2.03 m versus 0.89–1.19 m during the SW monsoon, a NE/SW H_s ratio of approximately 1.6–1.8 across the four sites (Table 4). At BT04, NE monsoon mean $H_s = 2.03$ m versus SW monsoon mean $H_s = 1.19$ m. The SW monsoon is, therefore, markedly milder than the NE monsoon in both wind forcing and sea state. Transition months (particularly April and May) exhibit the lowest wave heights of the year: mean H_s at BT04 drops to 0.88 m in April and 0.77 m in May, below any SW monsoon month.

These are candidate periods for subsequent threshold- and persistence-based operability assessment; operability is not quantified here against vessel-specific access thresholds. Figure 6 illustrates the seasonal wind–wave pattern at BT03 as a representative transitional-depth site.

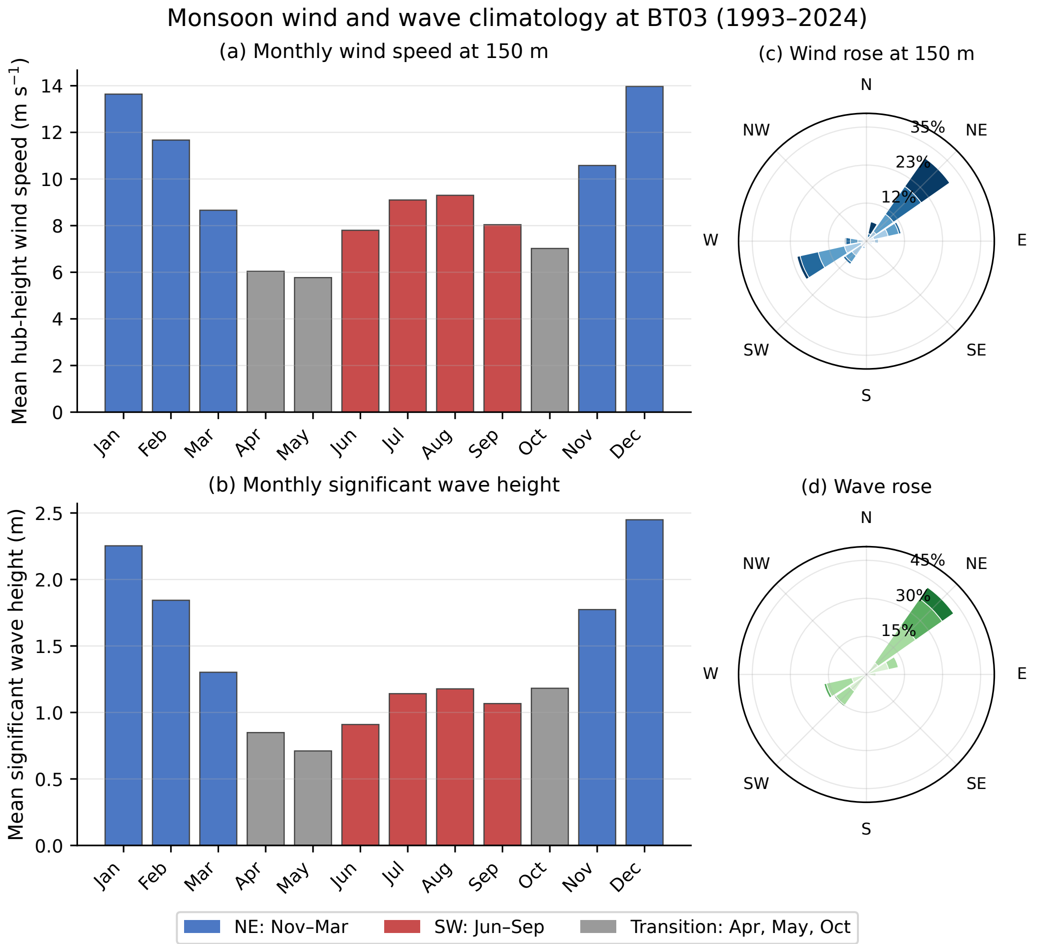

Figure 6. Monsoon wind and wave climatology at BT03, selected as a representative transitional-depth site. Monthly mean hub-height wind speed, monthly mean significant wave height, wind rose, and wave rose are computed from ERA5 data over 1993–2024. Bar colors indicate the NE monsoon (blue, November–March), SW monsoon (red, June–September), and transition months (grey, April, May, October), consistent with the data-driven seasonal classification described in Section 3.5. Wind and wave roses use the meteorological "from" direction convention.

3.6. Method-Based Sensitivity of Wind and Wave Screening

The baseline alpha replacement fraction is 0.22–0.51% across BT01–BT04; no calendar month required fallback beyond its site-specific monthly median. Across the bounded-hourly baseline, fixed $\alpha = 0.10$, fixed $\alpha = 1/7$, and alternative $[-0.10, 0.40]$ bounded-hourly cases, mean 150 m wind speed is 7.71–7.89, 9.04–9.31, 9.30–9.59, and 9.75–10.06 m s^{-1} at BT01–BT04, respectively. Gross 15 MW CF ranges are 46.70–48.63%, 57.52–59.72%, 58.56–60.72%, and 62.20–64.24%. The wind-resource order BT04–BT03–BT02–BT01 is invariant, so BT01 and BT04 remain clearly separated and the BT02–BT03 wind order is retained under these method cases.

Wave extraction is more consequential for the intermediate coordinates. Across nearest-valid, masked-bilinear, and inverse-distance methods, mean H_s ranges from 1.06–1.17 m (BT01), 1.22–1.28 m (BT02), 1.28–1.39 m (BT03), and 1.49–1.55 m (BT04); P95 ranges are 2.15–2.40, 2.61–2.75, 2.75–3.08, and 3.27–3.44 m. BT01 and BT04 remain invariant endpoint cases. BT02 and BT03 are identical under nearest-valid extraction but separate under the two weighted methods; their wave-exposure distinction is, therefore, extraction-method dependent. Supplementary Tables S1–S5 provide the alpha quality-control diagnostics, wind-extrapolation sensitivity, wave-grid corners and interpolation weights, wave-extraction method comparison, and combined screening scenarios. These are method-based sensitivity ranges, not statistical confidence intervals or a formal uncertainty budget; published ERA5 validation provides separate context rather than bounds on the present estimates.

3.7. Interannual Variability

Annual mean hub-height wind speed and gross single-turbine CF show moderate interannual variability over the 1993–2024 ERA5 record (Figure 7). COV of annual mean $\bar{V}_{\text{hub}}$ is 5.5–6.6%; COV of annual WPD is 10.6–13.7%; COV of annual gross single-turbine CF is 9.8–10.2% (Table 3) and COV of annual mean H_s is 5.8–6.5% (Figure 7). The roughly twofold amplification of the WPD COV relative to the wind-speed COV follows directly from the cubic dependence of power density on wind speed, which magnifies relative wind-speed anomalies. The 9.8–10.2% COV of annual gross CF indicates moderate interannual production variability at screening level; it characterizes interannual dispersion of the resource, not bankable revenue certainty.

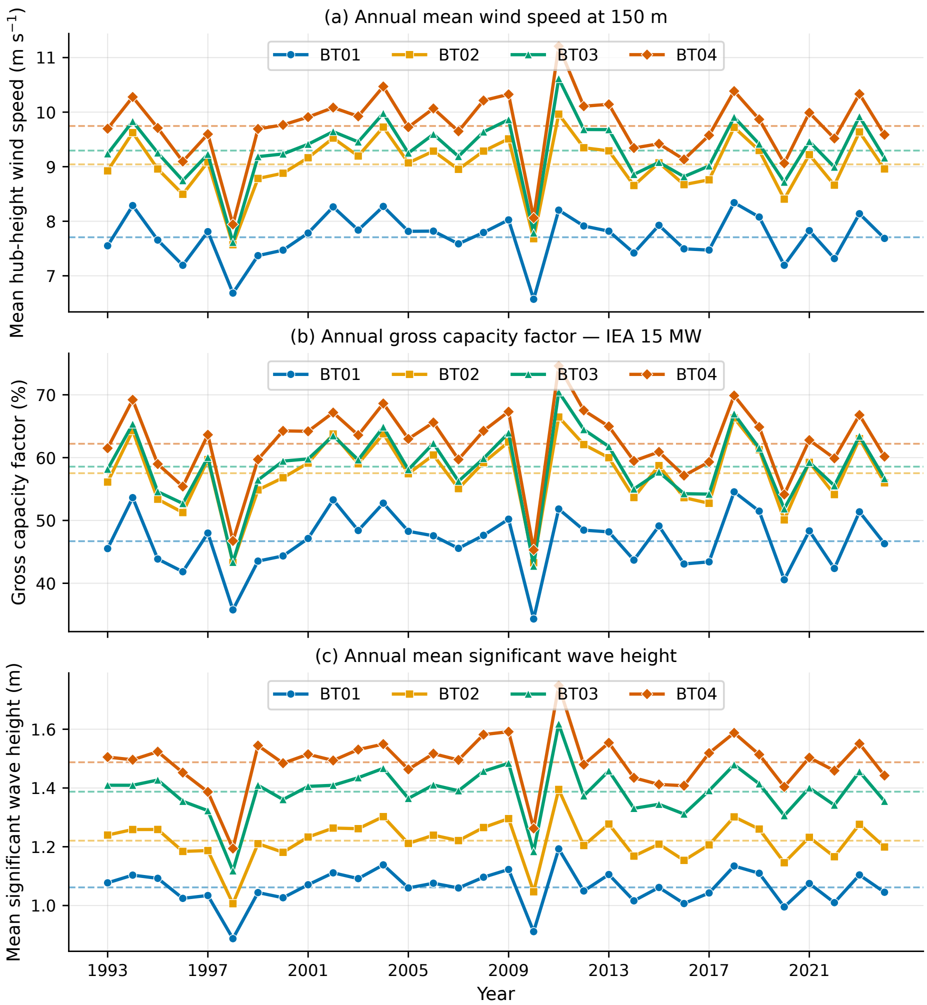

Figure 7. Interannual variability at BT01–BT04 over 1993–2024. (**a**) Annual mean hub-height (150 m) wind speed. (**b**) Annual gross single-turbine capacity factor for the IEA Wind 15 MW reference turbine. (**c**) Annual mean significant wave height. Dashed lines indicate the 32-year mean per site. Interannual COV of annual gross CF is 9.8–10.2%; COV of annual mean H_s is 5.8–6.5%.

3.8. Long-Term Trends and Change-Point Diagnostics

No statistically significant monotonic trend was detected at $\alpha = 0.05$ in annual mean V_{hub}, annual gross 15 MW CF, or annual mean H_{s} at any coordinate (Mann–Kendall $p = 0.530$–0.860, 0.711–0.948, and 0.910–0.962, respectively). Sen slopes were small and all 95% confidence intervals included zero. Pettitt tests likewise detected no significant change point ($p \geq 0.554$ for wind, $p \geq 0.737$ for CF, and $p \geq 0.901$ for waves). The complete tau, slope, confidence-interval, candidate-year, and p-value results are reported in Supplementary Table S6. These findings support only the statement that no monotonic trend or single change point was detected over 1993–2024; they do not prove stationarity.

3.9. Integrated Metocean Screening

Table 5 synthesizes the preceding results into an integrated screening matrix for the four representative sites. Under the present site configuration, gross single-turbine CF, gross AEP, and wave exposure all co-vary along the selected sequence, without implying an independent depth effect or domain-wide trend. BT04 achieves the highest gross single-turbine CF (62.20%) and gross AEP (81.7 $\mathrm{GWh\,yr^{-1}}$), but is simultaneously the deepest site (161 m, floating-suitable) and the most wave-exposed (mean $H_{\mathrm{s}} = 1.49$ m, max $H_{\mathrm{s}} = 6.34$ m). BT04 should, therefore, not be read simply as the "best" site: it is the highest-yield option but also the one with the greatest expected technical demand, requiring a floating substructure in the most exposed conditions. Conversely, BT01 should not be read simply as the "worst": its gross yield is the lowest (CF 46.70%), but it offers the most benign marine environment (27 m depth, mean $H_{\mathrm{s}} = 1.06$ m) and may carry nearshore logistical, cable-length, and grid-connection advantages that lie outside the scope of this screening. The BT02–BT03 pair illustrates a further screening insight: their gross CF values differ by only about one percentage point (57.52% versus 58.56%), while their depths (49 m versus 81 m) place them in different foundation classes. At such small gross-yield differences, foundation, geotechnical, and cost considerations may become more influential than the small difference in gross wind-resource indicators. Within the indicators considered here, no representative site combines the highest gross yield with the lowest water-depth and wave-exposure constraints; the screening matrix makes this coupling explicit.

Table 5. Integrated metocean screening matrix for the four representative sites. CF: gross single-turbine capacity factor (IEA Wind 15 MW, 150 m hub). $\mathrm{COV_{CF}}$: interannual coefficient of variation of annual CF. Foundation class based on GEBCO 2025 water depth. The matrix supports early-stage engineering prioritization only; no final site selection is made. The wind-resource ordering is invariant across the tested extrapolation cases. The BT02–BT03 wave-exposure distinction is extraction-method dependent and is not interpreted as robustly resolved.

Site	Depth (m)	$\bar{V}_{\mathrm{hub}}$ ($\mathrm{m\,s^{-1}}$)	CF (%)	$\mathrm{COV_{CF}}$ (%)	$\bar{H}_{\mathrm{s}}$ (m)	P95 H_{s} (m)	Foundation Class
BT01	27	7.71	46.70	10.23	1.06	2.15	Fixed (monopile)
BT02	49	9.04	57.52	9.88	1.22	2.61	Fixed (monopile/jacket)
BT03	81	9.30	58.56	10.18	1.39	3.08	Transitional (jacket/semi-sub)
BT04	161	9.75	62.20	9.83	1.49	3.27	Floating

3.10. Reference-Turbine Sensitivity

Gross single-turbine capacity factor and AEP for the four reference turbines are summarised in Table 6. This comparison should be interpreted as a reference-turbine sensitivity rather than as a pure turbine-size scaling exercise, because the four designs differ simultaneously in rated power, hub height, specific power, rated wind speed, and power-curve shape. Consequently, differences in CF cannot be attributed to rated capacity alone.

The lower-rated NREL 5 MW and DTU/IEA 10 MW turbines yield gross CF ranges of 38.05–56.63% and 38.07–56.31%, respectively, whereas the IEA 15 MW baseline yields 46.70–62.20%. These differences reflect the combined influence of hub height and turbine-specific power-curve characteristics rather than a simple capacity effect. By contrast, the gross CF of the IEA 22 MW reference turbine differs from that of the IEA 15 MW turbine by less than one percentage point at all four coordinates. At BT04, the two values are effectively identical, with 62.17% for the IEA 22 MW turbine and 62.20% for the IEA 15 MW turbine.

Although gross CF differs by less than one percentage point between the selected IEA 15 MW and 22 MW reference turbines, gross single-turbine AEP increases substantially because of the higher rated capacity. At BT04, for example, AEP increases from 81.74 to 119.81 GWh yr^{-1}, while CF remains nearly unchanged. This comparison is limited to gross single-turbine performance under the present ERA5-derived wind conditions and does not constitute a wind-farm-scale technical or economic assessment of turbine upscaling.

Table 6. Gross single-turbine capacity factor (CF, %) and AEP (GWh yr^{-1}) for four reference turbines at each screening site. IEA 15 MW is the manuscript baseline. All values are gross indicators (no losses). Hub heights: NREL 5 MW = 90 m, DTU 10 MW = 119 m, IEA 15 MW = 150 m, IEA 22 MW = 170 m [5].

Site	NREL 5 MW CF/AEP	DTU 10 MW CF/AEP	IEA 15 MW CF/AEP	IEA 22 MW CF/AEP
BT01	38.05/16.66	38.07/33.35	46.70/61.36	47.24/91.03
BT02	51.11/22.39	50.80/44.50	57.52/75.58	57.61/111.03
BT03	52.62/23.05	52.23/45.75	58.56/76.95	58.61/112.96
BT04	56.63/24.80	56.31/49.33	62.20/81.74	62.17/119.81

4. Discussion

4.1. Contribution Relative to Previous Vietnam Offshore Wind Studies

Previous assessments of offshore wind potential along the Vietnamese coast – national atlas products [28], WRF-based dynamical downscaling [25,27], and satellite-derived resource mapping—have established that the Binh Thuan–Phu Quy offshore domain holds high wind potential, but they characterize the resource at regional scale and in a single variable. What they do not provide is the multi-variable information that early engineering screening actually requires: how wind yield, water depth, wave exposure, seasonal operating environment, and interannual variability combine at specific candidate locations. The contribution of this study is, therefore, not another national-scale wind atlas, but a regional preliminary screening workflow evaluated at representative coordinates that combines wind yield, bathymetry, wave exposure, monsoon seasonality, and interannual variability at representative locations, using a consistent 32-year hourly ERA5 record, GEBCO 2025 bathymetry, and modern IEA reference turbine power curves. No claim is made of being the first assessment of offshore wind potential in the region; the advance lies in the integration and the regional, development-oriented screening framing; coordinate extraction does not add spatial information to the native ERA5 fields.

4.2. Sustainability Implications for Early Offshore Wind Planning

Maximizing wind yield alone is not a sufficient sustainability-oriented planning criterion. The selected sequence demonstrates why yield should be considered alongside water depth, indicative foundation demand, and marine exposure: the highest-yield coordinate is also the deepest and most exposed. Transparent early screening can direct limited surveys and planning effort toward better-matched alternatives and thereby support resource-efficient decision making. The open ERA5–GEBCO workflow is reproducible and comparatively low cost, which is useful in data-scarce emerging markets, and it provides inputs for later environmental, socio-economic, marine-spatial, lifecycle, and techno-economic assessment. The present study does not quantify lifecycle emissions, ecological effects, social acceptance, or project economics.

4.3. Coupled Energy-Yield, Wave-Exposure and Foundation-Depth Trade-Off

Along the selected BT01–BT04 sequence, wind resource, gross energy yield, water depth, and wave exposure increase together. Because location, distance from shore, coastal exposure, and depth vary simultaneously, this co-variation is not interpreted as a causal effect of depth or as a domain-wide relationship. Gross CF rises from BT01 (46.7%, 27 m) through BT02 (57.5%, 49 m) and BT03 (58.6%, 81 m) to BT04 (62.2%, 161 m), while P95 H_s increases from 2.15 m to 3.27 m; the largest hourly ERA5 H_s in the analyzed period also increases from 3.82 m to 6.34 m, although this record maximum is not a return-period design value. The practical consequence is that different, equally legitimate screening criteria select different sites. A wind-only ranking selects BT04 unambiguously. A ranking that gives greater weight to water-depth class, wave exposure, and near-term deployability may instead favor the shallower, less exposed sites, since at 161 m water depth BT04 requires a floating substructure—with substantially higher expected capital expenditure than bottom-fixed structures [7]—under the most exposed wave climate of the four representative sites. Gross capacity factor alone is, therefore, not a sufficient basis for site prioritization in this domain; the integrated screening makes the yield–depth–exposure trade-off explicit rather than allowing a single wind-resource metric to conceal it.

The BT02–BT03 comparison sharpens this point. The two sites are nearly indistinguishable in resource terms—gross CF of 57.5% versus 58.6% and gross AEP of 75.6 versus 77.0 GWh yr^{-1}—yet BT03 lies at 81 m depth against 49 m at BT02, implying a different indicative foundation class and greater depth-related design uncertainty. The screening-level implication is that the small gross-yield gain from BT02 to BT03 should not be interpreted as sufficient evidence for preferring the deeper site without further foundation, geotechnical, grid-access, and cost assessment. In such cases, the choice between candidate sites may be controlled more by foundation cost, geotechnical conditions, grid access, and construction logistics than by the small difference in gross wind-resource indicators. BT01, finally, illustrates the opposite pole of the trade-off: it has the lowest gross yield of the sequence, but also the shallowest water depth and the most benign wave climate, which may be relevant where nearshore logistics, cable length, or grid connectivity are binding constraints. The wave sensitivity further limits this comparison: BT02 and BT03 are identical under nearest-valid extraction and separate only under weighted interpolation. Their intermediate wave ranking is, therefore, not robust, while the BT01–BT04 endpoint contrast persists across all tested methods.

4.4. Monsoon Control of Production and Marine Operations

The NE monsoon (November–March) plays a dual role in this domain. It is the season of maximum wind resource—NE/SW hub-height wind speed ratios of 1.22–1.37, with monthly mean wind speed at BT04 reaching 12.02 m s^{-1} and directional resultant length $R > 0.80$ indicating a highly persistent regime—and simultaneously the season of strongest wave forcing, with NE/SW H_s ratios of approximately 1.6–1.8 (Table 4). The months that generate the largest share of annual energy are, therefore, also the months with the most energetic sea states and, plausibly, more constrained marine accessibility. This coincidence implies that future design and operational studies should evaluate energy production, structural load cases, and access constraints in a seasonally coupled manner rather than treating them as independent issues.

The SW monsoon (June–September) is markedly milder than the NE monsoon in both wind forcing ($R > 0.71$ at BT04) and sea state, and the transition months (April, May, and October) exhibit the weakest and least persistent wind forcing ($R < 0.55$ at BT04) together with the lowest wave heights of the year—mean H_s at BT04 falls to 0.88 m in April and 0.77 m in May. April and May have the lowest monthly mean sea states, whereas October is classified as transitional by wind direction but is not assumed to be climatologically equivalent. These monthly means do not constitute an operational weather-window analysis: actual operability depends on vessel- and activity-specific exceedance thresholds, persistence statistics, and logistics constraints, none of which are analyzed here.

4.5. Limitations and Interpretation of the Screening Results

The results must be interpreted within the scope of an early-stage screening built exclusively on publicly available reanalysis and global bathymetry. No offshore meteorological mast, floating LiDAR, wave buoy, ADCP/current-meter, or geotechnical dataset enters the analysis, and no bias correction is applied to ERA5. Consequently, the reported mean wind speeds, gross CF and AEP values, P95 wave heights, monsoon statistics, and depth-based site classes should be interpreted as regional screening indicators, not as validated design, financial, or bankable resource inputs.

Published station comparisons inform, but do not correct, this interpretation. Doan et al. [25] validated a 10 km WRF simulation against six Vietnamese island stations (2006–2015) and reported systematic positive near-surface wind-speed biases—largest ($3.5\ \mathrm{m\,s^{-1}}$) at Phu Quy Island—attributed mainly to unresolved small-island representation, with much closer agreement against QuikSCAT over open water (mean bias approximately $0.84\ \mathrm{m\,s^{-1}}$). These findings indicate that gridded products can overestimate winds at small-island stations while performing better over open water; they are used here solely for uncertainty interpretation. Applying them as a deterministic correction to ERA5 hub-height winds at the offshore screening sites BT01–BT04 would not be justified.

Three further boundaries define the scope. First, all CF and AEP values are gross, single-turbine quantities based on reference power curves; they exclude wake, electrical, availability, curtailment, degradation, and wind-farm layout effects, and the 46.7–62.2% CF range should not be read as expected operational wind-farm capacity factors. Second, P95 H_s is a long-term climate percentile, not a return-period extreme. Third, the study performs no extreme-value analysis, environmental contour development, ocean current characterization, wind–wave–current misalignment analysis, geotechnical assessment, or formal IEC design load case definition for fixed or floating systems [36,37]. The Mann–Kendall/Sen and Pettitt diagnostics detected no significant monotonic trend or single change point, respectively. COV remains a dispersion metric and neither result proves stationarity. Method-based sensitivity ranges, statistical confidence intervals for Sen slope, and published ERA5 validation context are not interchangeable. These analyses constitute the necessary next stage for any site progressing from regional screening toward preliminary engineering design.

5. Conclusions

This study presented a 32-year (1993–2024) integrated wind–wave–bathymetry metocean screening of four representative offshore wind sites (BT01–BT04) in the Binh Thuan–Phu Quy offshore domain, Vietnam, based on hourly ERA5 reanalysis, GEBCO 2025 bathymetry, and reference turbine power curves. The analysis is an early-stage engineering screening: it is not a bankable resource assessment and does not constitute a design basis.

Along the selected BT01–BT04 coordinate sequence, mean hub-height (150 m) wind speed increases from 7.71 to 9.75 m s^{-1}, gross single-turbine capacity factor for the IEA Wind 15 MW reference turbine from 46.7% to 62.2%, and gross annual energy production from 61.4 to 81.7 GWh yr^{-1}. Over the same sequence, mean significant wave height increases from 1.06 to 1.49 m and P95 H_s from 2.15 to 3.27 m. For the selected IEA 15 MW and 22 MW reference designs, gross CF differs by less than one percentage point; this reflects combined hub-height and power-curve differences and is not a general turbine-upscaling assessment.

Along the selected BT01–BT04 sequence, wind resource, gross energy yield, water depth, and wave exposure increase together; this co-variation is not a causal depth relationship or a domain-wide trend. BT04 is the highest-yield site but also the deepest (161 m, floating-suitable) and the most wave-exposed, implying the most demanding combination of water-depth and wave-exposure indicators among the four screening sites. BT01 is the lowest-yield site but offers the shallowest water depth and the most benign wave climate. BT02 and BT03 occupy intermediate positions with nearly identical gross capacity factors (57.5% versus 58.6%) despite belonging to different depth and indicative foundation classes (49 m versus 81 m). At such small yield differences, foundation, geotechnical, grid-access, and cost considerations may become more influential than the small difference in gross wind-resource indicators. Within the indicators considered here, no representative site combines the highest gross yield with the lowest water-depth and wave-exposure constraints.

Seasonally, a data-driven classification identifies the northeast monsoon (November–March) as the dominant season for both wind resource and wave forcing, the southwest monsoon (June–September) as markedly milder, and the transition months (April, May, October)—particularly April and May—as having the lowest wave heights of the year. Monthly mean sea states do not define operational weather windows, which require threshold-exceedance and persistence analysis. Interannual variability is moderate at screening level: the coefficient of variation of annual gross capacity factor is 9.8–10.2% and that of annual mean significant wave height is 5.8–6.5% across the four sites. No statistically significant monotonic trend or Pettitt change point was detected for annual mean hub-height wind, gross 15 MW CF, or annual mean H_s at any coordinate over 1993–2024. This does not prove stationarity.

The screening relies exclusively on reanalysis and global bathymetry, without offshore mast, LiDAR, buoy, current, or geotechnical measurements and without ERA5 bias correction; all reported values are regional screening indicators. Progression from screening toward engineering design requires extreme-value analysis of wind speed and H_s, environmental contour development, ocean current characterization, wind–wave–current misalignment assessment, geotechnical investigation, and formal IEC design load case development for fixed and floating systems. The central message for practice is that early offshore wind prioritization in the Binh Thuan–Phu Quy offshore domain should integrate wind yield, bathymetry, wave climate, monsoon seasonality, and interannual variability, rather than relying on wind resource alone. From a sustainability perspective, this open-data integration supports transparent and resource-efficient allocation of early survey and planning effort, while lifecycle, ecological, social, and economic sustainability remain outside the quantified scope and require dedicated subsequent assessment.

Supplementary Materials: The following supporting information can be downloaded at: https://www.mdpi.com/article/10.3390/su18157971/s1, Table S1: Alpha quality-control diagnostics by coordinate; Table S2: Wind extrapolation method sensitivity; Table S3: ERA5 wave-grid corners, validity, and interpolation weights; Table S4: Wave extraction method comparison; Table S5: Combined method-based screening sensitivity and separate rankings; Table S6: Trend and change-point diagnostics.

Author Contributions: Conceptualization, T.D.P. and D.V.T.; methodology, T.D.P.; software, T.D.P. and D.M.L.; formal analysis, T.D.P. and T.B.D.; investigation, T.D.P., D.V.T. and P.Q.N.; data curation, T.D.P. and D.M.L.; writing—original draft preparation, T.D.P.; writing—review and editing, T.B.D., D.M.L., D.V.T., P.Q.N. and D.T.N.; visualization, D.M.L.; supervision, D.T.N. and P.Q.N.; project administration, T.D.P. All authors have read and agreed to the published version of the manuscript.

Funding: This project is partly funded by the European Union, under Grant Agreement No 101232814 via GREENSEA project. Views and opinions expressed are, however, those of the author(s) only and do not necessarily reflect those of the European Union. Neither the European Union nor the granting authority can be held responsible for them.

Institutional Review Board Statement: Not applicable.

Informed Consent Statement: Not applicable.

Data Availability Statement: The processed coordinate-specific statistics and analysis scripts are available from the corresponding author upon reasonable request.

Acknowledgments: ERA5 reanalysis data were obtained from the Copernicus Climate Change Service (C3S) Climate Data Store. GEBCO 2025 bathymetry was obtained from the General Bathymetric Chart of the Oceans (GEBCO; https://www.gebco.net (accessed on 9 July 2026)). IEA Wind reference turbine power curves were obtained from the respective open-source repositories cited in the manuscript.

Conflicts of Interest: The authors declare no conflicts of interest.

References

1. Global Wind Energy Council (GWEC). *Global Offshore Wind Report 2024*; GWEC: Brussels, Belgium, 2024. Available online: https://wfo-global.org/wp-content/uploads/2025/04/WFO_Global-Offshore-Wind-Report-2024_final.pdf (accessed on 9 July 2026).
2. Soares-Ramos, E.; de Oliveira-Assis, L.; Sarrias-Mena, R.; Fernández-Ramírez, L. Current status and future trends of offshore wind power in Europe. *Energy* **2020**, *202*, 117787. [CrossRef]
3. Diaconita, A.; Andrei, G.; Rusu, L. An overview of the offshore wind energy potential for twelve significant geographical locations across the globe. *Energy Rep.* **2022**, *8*, 194–201. [CrossRef]
4. Gaertner, E.; Rinker, J.; Sethuraman, L.; Zahle, F.; Anderson, B.; Barter, G.; Abbas, N.; Meng, F.; Bortolotti, P.; Skrzypinski, W.; et al. *Definition of the IEA Wind 15-Megawatt Offshore Reference Wind Turbine*; Technical Report NREL/TP-5000-75698; National Renewable Energy Laboratory: Golden, CO, USA, 2020. [CrossRef]
5. Zahle, F.; Barlas, A.; Lønbæk, K.; Bortolotti, P.; Zalkind, D.; Wang, L.; Labuschagne, C.; Sethuraman, L.; Barter, G. *Definition of the IEA Wind 22-Megawatt Offshore Reference Wind Turbine*; DTU Wind Energy Report E-0243 IEA Wind TCP Task 55; Technical University of Denmark: Lyngby, Denmark, 2024. [CrossRef]
6. Veers, P.; Dykes, K.; Lantz, E.; Barth, S.; Bottasso, C.L.; Carlson, O.; Clifton, A.; Green, J.; Green, P.; Holttinen, H.; et al. Grand challenges in the science of wind energy. *Science* **2019**, *366*, eaau2027. [CrossRef] [PubMed]
7. Díaz, H.; Guedes Soares, C. Review of the current status, technology and future trends of offshore wind farms. *Ocean Eng.* **2020**, *209*, 107381. [CrossRef]
8. Jung, C.; Schindler, D. The role of the power law exponent in wind energy assessment: A global analysis. *Int. J. Energy Res.* **2021**, *45*, 8484–8496. [CrossRef]
9. Carta, J.; Ramírez, P.; Velázquez, S. A review of wind speed probability distributions used in wind energy analysis: Case studies in the Canary Islands. *Renew. Sustain. Energy Rev.* **2009**, *13*, 933–955. [CrossRef]
10. Khan, M.; Ahmed, M. Bayesian method for estimating Weibull parameters for wind resource assessment in a tropical region: A comparison between two-parameter and three-parameter Weibull distributions. *Wind Energy Sci.* **2023**, *8*, 1277–1298. [CrossRef]
11. Pryor, S.C.; Shepherd, T.J.; Barthelmie, R.J. Interannual variability of wind climates and wind turbine annual energy production. *Wind Energy Sci.* **2018**, *3*, 651–665. [CrossRef]
12. Wen, Y.; Kamranzad, B.; Lin, P. Assessment of long-term offshore wind energy potential in the south and southeast coasts of China based on a 55-year dataset. *Energy* **2021**, *224*, 120225. [CrossRef]
13. Hersbach, H.; Bell, B.; Berrisford, P.; Hirahara, S.; Horányi, A.; Muñoz-Sabater, J.; Nicolas, J.; Peubey, C.; Radu, R.; Schepers, D.; et al. The ERA5 global reanalysis. *Q. J. R. Meteorol. Soc.* **2020**, *146*, 1999–2049. [CrossRef]
14. Soci, C.; Hersbach, H.; Simmons, A.; Poli, P.; Bell, B.; Berrisford, P.; Horanyi, A.; Munoz-Sabater, J.; Nicolas, J.; Radu, R.; et al. The ERA5 global reanalysis from 1940 to 2022. *Q. J. R. Meteorol. Soc.* **2024**, *150*, 4014–4048. [CrossRef]
15. Olauson, J. ERA5: The new champion of wind power modelling? *Renew. Energy* **2018**, *126*, 322–331. [CrossRef]

16. Gualtieri, G. Analysing the uncertainties of reanalysis data used for wind resource assessment: A critical review. *Renew. Sustain. Energy Rev.* **2022**, *167*, 112741. [CrossRef]
17. Castro-Santos, L.; Silva, D.; Bento, A.; Salvação, N.; Guedes Soares, C. Economic feasibility of floating offshore wind farms in Portugal. *Ocean Eng.* **2020**, *207*, 107393. [CrossRef]
18. Allen, C.; Viscelli, A.; Dagher, H.; Goupee, A.; Gaertner, E.; Abbas, N.; Hall, M.; Barter, G. *Definition of the UMaine VolturnUS-S Reference Platform Developed for the IEA Wind 15-Megawatt Offshore Reference Wind Turbine*; Technical Report NREL/TP-5000-76773; National Renewable Energy Laboratory: Golden, CO, USA, 2020.
19. Wang, J.; Liu, J.; Wang, Y.; Liao, Z.; Sun, P. Spatiotemporal variations and extreme value analysis of significant wave height in the South China Sea based on 71-year long ERA5 wave reanalysis. *Appl. Ocean Res.* **2021**, *113*, 102750. [CrossRef]
20. Tercan, E.; Tapkın, S.; Latinopoulos, D.; Dereli, M.; Tsiropoulos, A.; Ak, M. A GIS-based multi-criteria model for offshore wind energy power plants site selection in both sides of the Aegean Sea. *Environ. Monit. Assess.* **2020**, *192*, 652. [CrossRef] [PubMed]
21. Tavares, L.; Shadman, M.; Assad, L.; Silva, C.; Landau, L.; Estefen, S. Assessment of the offshore wind technical potential for the Brazilian Southeast and South regions. *Energy* **2020**, *196*, 117097. [CrossRef]
22. Wang, C.N.; Nguyen, N.; Dang, T.T. Offshore wind power station (OWPS) site selection using a two-stage MCDM-based spherical fuzzy set approach. *Sci. Rep.* **2022**, *12*, 4260. [CrossRef] [PubMed]
23. Government of Vietnam. *Decision No. 500/QD-TTg Dated 15 May 2023 Approving the National Power Development Plan for 2021–2030 with a Vision to 2050 (PDP8)*; Government of Vietnam: Hanoi, Vietnam, 2023.
24. Government of Vietnam. *Decision No. 768/QD-TTg Dated 15 April 2025 Approving the Revision of the National Power Development Plan for 2021–2030 with a Vision to 2050 (Revised PDP8)*; Government of Vietnam: Hanoi, Vietnam, 2025.
25. Doan, V.; Dinh, V.; Kusaka, H.; Cong, T.; Khan, A.; Du, V.; Duc, N. Usability and challenges of offshore wind energy in Vietnam revealed by the regional climate model simulation. *SOLA* **2019**, *15*, 113–118. [CrossRef]
26. Quang, V.; Doan, V.; Dinh, V.; Nguyen, N.; Du, T.; Cong, T. Evaluation of resource spatial-temporal variation, dataset validity, infrastructures and zones for Vietnam offshore wind energy. *Vietnam J. Sci. Technol. Eng.* **2020**, *62*, 3–16. [CrossRef]
27. Tuy, S.; Lee, H.; Chreng, K. Integrated assessment of offshore wind power potential using Weather Research and Forecast (WRF) downscaling with Sentinel-1 satellite imagery, optimal sites, annual energy production and equivalent CO_2 reduction. *Renew. Sustain. Energy Rev.* **2022**, *163*, 112501. [CrossRef]
28. National Centre for Hydro-Meteorological Forecasting (NCHMF); United Nations Development Programme (UNDP); Norwegian Meteorological Institute. *Assessment of the Technical Potential of Offshore Wind Energy in Viet Nam*; UNDP Viet Nam: Hanoi, Vietnam, 2025. Available online: https://www.undp.org/vietnam/publications/assessment-technical-potential-offshore-wind-energy-viet-nam (accessed on 9 July 2026).
29. Doan, V.; Kusaka, H.; Du, T.; Nguyen, D.; Cong, T. Numerical approach for studying offshore wind power potential along the southern coast of Vietnam. In *Proceedings of the 1st Vietnam Symposium on Advances in Offshore Engineering (VSOE 2018)*; Lecture Notes in Civil Engineering; Randolph, M., Doan, D., Tang, A., Bui, M., Dinh, V., Eds.; Springer: Singapore, 2019; Volume 18. [CrossRef]
30. Dinh, Q.; Doan, Q.; Ngo-Duc, T.; Dinh, V.; Duc, N. Offshore wind resource in the context of global climate change over a tropical area. *Appl. Energy* **2022**, *308*, 118369. [CrossRef]
31. He, J.; Chan, P.; Li, Q.; Tong, H. Mapping future offshore wind resources in the South China Sea under climate change by regional climate modeling. *Renew. Sustain. Energy Rev.* **2023**, *188*, 113865. [CrossRef]
32. Tung, T.; Chien, N. An assessment of potential wave power along a coastal province, Central Vietnam. *Int. Mar. Energy J.* **2023**, *6*, 27–35. [CrossRef]
33. Jonkman, J.; Butterfield, S.; Musial, W.; Scott, G. *Definition of a 5-MW Reference Wind Turbine for Offshore System Development*; Technical Report NREL/TP-500-38060; National Renewable Energy Laboratory: Golden, CO, USA, 2009. [CrossRef] [PubMed]
34. Bak, C.; Zahle, F.; Bitsche, R.; Kim, T.; Yde, A.; Henriksen, L.; Hansen, M.; Blasques, J.; Gaunaa, M.; Natarajan, A. The DTU 10-MW Reference Wind Turbine, 2013. In Proceedings of the Danish Wind Power Research 2013, Fredericia, Denmark, 27–28 May 2013.
35. GEBCO Compilation Group. GEBCO 2025 Grid. In *General Bathymetric Chart of the Oceans*; GEBCO Compilation Group: Liverpool, UK, 2025. [CrossRef]
36. *IEC 61400-3-1*; Wind Energy Generation Systems—Part 3-1: Design Requirements for Fixed Offshore Wind Turbines. International Electrotechnical Commission: Singapore, 2019.
37. *IEC 61400-3-2*; Wind Energy Generation Systems—Part 3-2: Design Requirements for Floating Offshore Wind Turbines. International Electrotechnical Commission: Singapore, 2025.
38. To Duy, T.; Herrmann, M.; Estournel, C.; Marsaleix, P.; Duhaut, T.; Bui Hong, L.; Trinh Bich, N. The role of wind, mesoscale dynamics, and coastal circulation in the interannual variability of the South Vietnam Upwelling, South China Sea—Answers from a high-resolution ocean model. *Ocean Sci.* **2022**, *18*, 1131–1161. [CrossRef]
39. Ngo, T.; Hsin, Y.C. Impacts of wind and current on the interannual variation of the summertime upwelling off southern Vietnam in the South China Sea. *J. Geophys. Res. Ocean.* **2021**, *126*, e2020JC016892. [CrossRef]

40. Bell, B.; Hersbach, H.; Simmons, A.; Berrisford, P.; Dahlgren, P.; Horányi, A.; Muñoz-Sabater, J.; Nicolas, J.; Radu, R.; Schepers, D.; et al. The ERA5 global reanalysis: Preliminary extension to 1950. *Q. J. R. Meteorol. Soc.* **2021**, *147*, 4186–4227. [CrossRef]
41. Wang, J.; Wang, Y. Evaluation of ERA5 wave parameters with in situ data in the South China Sea. *Atmosphere* **2022**, *13*, 935. [CrossRef]